This article has been accepted for inclusion in a future issue of this journal. Content is final as presented, with the exception of pagination.

Adaptive Convex Loss Mappings for Enhanced Loss Assessment in Asynchronous Drives

Arne De Keyser, Hendrik Vansompel, and Guillaume Crevecoeur

***Abstract*— Control topologies in electric drive applications commonly aim at minimizing the dissipated power in the system to guarantee energy-efficient operation. Especially in vehicle electrification, loss minimization is the main objective in the supervisory control loops as this is directly related to the range of the vehicle. Advanced drive systems are characterized by an elevated complexity but require nevertheless a real-time control strategy to be implemented. Appropriate model abstraction, enabling real-time viability with a reliable system representation, is found in convex mapping procedures of the dissipated power in the drive components. These reduced-order models are generally obtained based on model information solely. This paper proposes a methodology to recursively enhance the reliability of the convex loss approximations. An instantaneous power flow estimation is assessed based on a unification of model expectations and sensor data. Using this information, a proper adaptation to the underlying convex loss coefficients is then determined. The methodology is validated in simulation for an electric drive on three different case studies. The algorithm is furthermore applied on actual experimental data of an asynchronous drive for validation purposes. Preliminary results demonstrate that the error on the loss assessment is reduced by 55.7%–89.0%. Adaptive convex loss mappings can, therefore, be consulted in practical control structures to ameliorate the reliability of loss minimization control schemes, while still maintaining a computationally efficient format.**

***Index Terms*— Adaptive models, convex mappings, electric drives, loss minimization, recursive estimation, systems modeling.**

I. Introduction

STATE-of-the-art control structures in electric drive technology often revolve around energy-efficient operation. Particularly in the automotive domain, the optimal energy management is a major concern, as the power losses are directly linked to the battery usage, and consequently the operational range, of hybrid or all-electric vehicles [1], [2]. This loss optimization is both tackled at the component level [3] and the level of supervisory control loops [4]. Nevertheless, contemporary drive systems impose ever increasing demands with respect to complexity of the decision-making agents [5] and real-time viability [6].

High-fidelity control strategies, such as model predictive control [5] and dynamic programming [7], provide a means to tackle dynamic problems and regulate the energy flow in the system in an optimal fashion. These methods are nevertheless time consuming, and therefore, less favorable for implementation in a real-time context, especially when facing high-dimensional problems. Dedicated and reduced-order heuristics need to be consulted to render these complex problems tractable [8], [9]. As the occurring losses constitute the focal point of the intended strategies, a more efficient representation is found in convex loss mappings [10]. The physical system is casted into a convex representation solely based on the power flows in the system. The detailed dynamic behavior is hereby abstracted. A convex loss formulation allows the control algorithm to rely on time-efficient convex optimization, significantly reducing the burden on the computational platform while maintaining a sufficient accuracy [11], [12].

A basic assumption in this approach is the availability of reliable model information, as the convex reformulations are constructed in advance based on the system model solely. The accessible model characteristics are nevertheless prone to imperfections. Moreover, reliable control should be guaranteed in uncertain and highly dynamic operating conditions [13]. Several filtering techniques coexist to unify model expectations with sensor interpretation [14], [15], focusing on the state variables. Although indirect information concerning the instantaneous power flows in the drive can be extracted, no thorough research has been conducted on the impact of combining measurement and model information in dynamically adaptable convex loss mappings. Changing characteristics are consequently compensated for in an automated fashion, inherently leading to an improved control in terms of energy dissipation.

In this paper, an adaptive approach to the convex reformulation of underlying loss mechanisms is proposed, combining the time-efficient model abstraction with the possibility to be equipped in flexible environments. A recursive scheme is derived based on an estimation of the instantaneous power flows in the system and the level of confidence in the current convex approximation. The introduced methodology is evaluated on the case study of a simplified asynchronous drive, represented in Fig. 1, subject to distinct imposed

Manuscript received February 22, 2018; accepted May 23, 2018. Manuscript received in final form May 30, 2018. This work was supported in part by Flanders Make, the strategic research centre for the manufacturing industry, through the Projects EVIT and EMODO, in part by BOF under Grant 01N02716, and in part by FWO under Research Project G.0D93.16N. Recommended by Associate Editor A. Chiuso. *(Corresponding author: Arne De Keyser.)*

The authors are with the Department of Electrical Energy, Metals, Mechanical Constructions and Systems, Ghent University, 9000 Ghent, Belgium, and also with EEDT-DC, Flanders Make, 3920 Lommel, Belgium (e-mail: arndkeys.dekeyser@ugent.be; hendrik.vansompel@ugent.be; guillaume.crevecoeur@ugent.be).

Color versions of one or more of the figures in this paper are available online at http://ieeexplore.ieee.org.

Digital Object Identifier 10.1109/TCST.2018.2843331

1063-6536 © 2018 IEEE. Personal use is permitted, but republication/redistribution requires IEEE permission.
See http://www.ieee.org/publications_standards/publications/rights/index.html for more information.

This article has been accepted for inclusion in a future issue of this journal. Content is final as presented, with the exception of pagination.

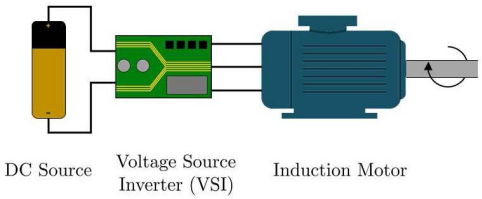

Fig. 1. Graphical overview of the studied asynchronous drive with controlled speed load.

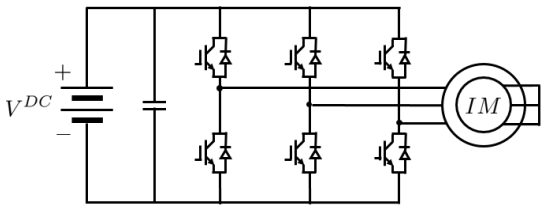

Fig. 2. Equivalent electric circuit of the considered drivetrain.

speed profiles. The system encompasses a dc voltage source, a power electronic inverter, and a single induction motor.

Prior to possible hardware implementations, the viability of the introduced framework is numerically analyzed for distinct dynamic loads. The capability of the approach to predict the occurring system losses by an adaptable convex model is, therefore, determined in both a simulation and an experimental environment. In the future applications, the convex loss models can provide a tool for supervisory control loops to enhance the system operation in terms of loss minimization, and hence, contribute to further advancements in contemporary control technology. Actuation of the complete system is then executed based on a decision-making agent relying on the available loss mapping information.

In Section II, a brief discussion of the dynamic system model is provided to describe the governing equations. The transition from the state estimation, using a slightly adapted Kalman filter, toward recursive power estimation is furthermore clarified. In Section III, the convex loss mappings are introduced and linked to the previously defined power flow estimations in order to obtain an adaptive formulation of the abstracted mappings. As the convex approximations are only constructed at discrete speeds, a heuristic approach to implement the methodology in a continuous environment is proposed in Section IV. The complete numerical procedure is then finally validated in simulation and based on collected experimental data in Section V.

II. Estimation of the Instantaneous Power Variables

The system under study is constructed by a series connection of a constant dc voltage source V^{dc} providing power to the input of a voltage source inverter, which is assumed to be an ideal component without losses or internal delays. In the future research, empirical models could nevertheless be introduced to capture the dissipation in the power electronic elements. The corresponding three-phase output system constitutes the supply for an induction motor. The equivalent electric circuit is provided in Fig. 2.

The dynamic behavior of the system is modeled, together with a simplified measurement equation in which the current in the system is assumed to be directly sensed by, possibly non-ideal, external equipment. An appropriate recursive estimation procedure is then carried out so as to provide the foundations for a reliable assessment of the instantaneous power flow variables in the considered system. In the remainder of this paper, the vector of state variables is consistently denoted by x, whereas the characteristic parameter set of the system is represented by the notation w. The system parameters are furthermore prone to uncertainty.

A. Dynamic Evolution of the Drivetrain

In order to estimate the power dissipation, the dynamic evolution of the system needs to be assessed first. A continuous representation of the studied electric drive as a function of the rotational speed Ω, the dynamically evolving state vector $x(t)$, and the input $u(t)$, is given as

$$\dot{x}(t) = A(\Omega, t)x(t) + B(t)u(t). \tag{1}$$

The speed dependence of the system matrix necessitates a linearization around the operating point, where the electric transients occur with a faster time constant than the evolution of the rotational speed. The dynamic behavior is expressed as a 4-D state-space system [16], with the state vector composed of the components of current and flux in the complex plane (i^{sx}, i^{sy}, ψ^{sx}, and ψ^{sy}). The time evolution is furthermore governed by the stator resistance R^s, rotor resistance R^r, stator inductance L^s, rotor inductance L^r, the mutual inductance L^m, and the number of pole pairs N^p of the asynchronous machine. The discrete state of the inverter switching elements is represented by the vector $x^b(t) \in \{0, 1\}^{3x1}$, whereas the vector u encompasses the real and imaginary parts of the stator voltage vector in the stationary stator frame, v^{sx} and v^{sy}, respectively. The rotor phases are hereby assumed to be short-circuited (2), as shown at the top of the next page. The symbol N is hereby engaged to shorten the notation

$$N = L^{m^2} - L^r L^s. \tag{3}$$

Based on the actual switching state and the dc voltage V^{dc}, the input vector is defined as

$$u(t) = \begin{bmatrix} \frac{2}{3} & -\frac{1}{3} & -\frac{1}{3} \\ 0 & \frac{\sqrt{3}}{3} & -\frac{\sqrt{3}}{3} \end{bmatrix} \begin{bmatrix} \frac{2}{3} & -\frac{1}{3} & -\frac{1}{3} \\ -\frac{1}{3} & \frac{2}{3} & -\frac{1}{3} \\ -\frac{1}{3} & -\frac{1}{3} & \frac{2}{3} \end{bmatrix} x^b(t)\, V^{\mathrm{dc}}$$
$$\triangleq T^{xy} T^n x^b(t)\, V^{\mathrm{dc}}. \tag{4}$$

The matrix T^{xy} transforms the voltage signals to the stationary frame, whereas T^n expresses the output voltage levels of the inverter as line-to-neutral voltages. Discretizing the system and introducing the discrete time index k by employing

This article has been accepted for inclusion in a future issue of this journal. Content is final as presented, with the exception of pagination.

$$A(\Omega,t)=\begin{bmatrix}\dfrac{L^rR^s+L^sR^r}{N} & -N^p\Omega(t) & -\dfrac{R^r}{N} & -\dfrac{L^rN^p}{N}\Omega(t)\\ N^p\Omega(t) & \dfrac{L^rR^s+L^sR^r}{N} & \dfrac{L^rN^p}{N}\Omega(t) & -\dfrac{R^r}{N}\\ -R^s & 0 & 0 & 0\\ 0 & -R^s & 0 & 0\end{bmatrix}$$

$$B(t)=\begin{bmatrix}-\dfrac{L^r}{N} & 0\\ 0 & -\dfrac{L^r}{N}\\ 1 & 0\\ 0 & 1\end{bmatrix} \tag{2}$$

a forward finite differencing method results in an equivalent system in discrete time; if the time step Δt is not too coarse

$$\begin{aligned}x_{k+1}&=\left(I+\Delta t\,A^c(t_k)+\Delta t\,A_k^{\Omega}(t_k)\Omega_k\right)x_k+\Delta t\,B(t_k)u_k(t_k)\\&\triangleq A_kx_k+B_ku_k.\end{aligned} \tag{5}$$

The definitions of the distinct matrices in this expression can be readily deduced based on a comparison with (2). The matrix $A(\Omega,t)$ is hereby written as the sum of a constant and a speed-dependent term containing the matrix entries in $\Omega(t)$, A^c, and A^{Ω}, respectively,

$$A(\Omega,t)=A^c(t)+A^{\Omega}(\Omega,t)\Omega(t). \tag{6}$$

Note that the matrix A^c only relies on the electrical parameters of the machine, which may nevertheless change over time. In order to complete the system representation, a measurement equation needs to be added, denoting the relation between state variables x_k and measured data y_k at time instant t_k. It is assumed that sensor information is available for the stator current components, disturbed by a Gaussian white noise signal v_k with covariance V_k. This nevertheless implies an estimation of the flux based on the model solely. Therefore,

$$y_k=C_kx_k+v_k. \tag{7}$$

As the stator phase currents are directly measured instead of the projections in the xy-frame, the measurement matrix C_k is given as

$$C_k=\begin{bmatrix}1 & 0 & 0 & 0\\ -\dfrac{1}{2} & \dfrac{\sqrt{3}}{2} & 0 & 0\\ -\dfrac{1}{2} & -\dfrac{\sqrt{3}}{2} & 0 & 0\end{bmatrix}. \tag{8}$$

B. Estimation of the State Variables

The previously incorporated models rely on the actual values of both state variables x_k and decisive model parameters w_k. However, these data are in practical applications that are not available and control of the drive is to be carried out based on expected values for the system characteristics. Errors in the model expectations thus mainly stem from uncertainty on and resulting deviations of the underlying physical parameters. As no measurement information about the stator flux components is available, a Kalman filter is implemented to recursively estimate the state variables using the proposed dynamical model [17]. Throughout this paper, estimations are consistently denoted by a hat on the corresponding symbol, whereas the respective error variable is denoted by the notation ξ ($\xi_k^{\bullet}=\bullet_k-\hat{\bullet}_k$).

Due to the inherent stochastic nature of the electric parameters, only known up to a prescribed tolerance, the system matrices A_k^c, A_k^{Ω}, and B_k are assumed to be stochastic as well. As discussed in [16], the elements of both matrices are incorporated in a single parameter set w_k

$$w_k=\begin{bmatrix}A_{k-1}^{c(1,1)} & \dots & A_{k-1}^{\Omega(1,1)} & \dots & B_{k-1}^{(1,1)} & \dots & B_{k-1}^{(4,2)}\end{bmatrix}^T. \tag{9}$$

The given parameter set is furthermore characterized by the constant associated covariance matrix X^w, whereas the uncertainty on the state variables over time is denoted by the matrix X_k^x. If input deviations are neglected, the dynamic equation of the system (5) can thus be written in a linearized representation with a quadratic error term $\mathcal{O}(\xi^2)$

$$\begin{aligned}x_{k+1}&=\left(\hat{A}_k+\xi_k^A\right)\left(\hat{x}_k+\xi_k^x\right)+\left(\hat{B}_k+\xi_k^B\right)u_k\\&=\hat{A}_k\hat{x}_k+\hat{B}_ku_k+\xi_k^A\hat{x}_k+\xi_k^Bu_k+\mathcal{O}(\xi^2)\\&\triangleq\hat{A}_k\hat{x}_k+\hat{B}_ku_k+G_{k+1}^{x,w}\xi_k^w+\mathcal{O}(\xi^2).\end{aligned} \tag{10}$$

The output relation (7) is assumed to be exactly known. The corresponding filtering scheme is then formulated, taking the influence of modeling errors into account but not altering the underlying dynamical model [16]. The optimal Kalman gain matrix K_k^x is defined to minimize the expected uncertainty on the state estimates. In the prediction step, an uncorrected estimate is provided based on the available modeling information and prior estimates. Afterward, the states are updated using the latest sensor data, significantly improving the estimation accuracy

$$\begin{aligned}\textit{Prediction}\quad \hat{x}_k^-&=\hat{A}_{k-1}\hat{x}_{k-1}+\hat{B}_{k-1}u_{k-1}\\X_k^{x^-}&=\hat{A}_{k-1}X_{k-1}^x\hat{A}_{k-1}^T+G_{k-1}^{x,w}W_{k-1}G_{k-1}^{x,w^T}\end{aligned}$$

This article has been accepted for inclusion in a future issue of this journal. Content is final as presented, with the exception of pagination.

$$\begin{aligned} \textit{Update} \quad & R_k^x = C_k X_k^{x^-} C_k^T + V_k \\ & K_k^x = X_k^{x^-} C_k^T R_k^{x^{-1}} \\ & \hat{x}_k = \hat{x}_k^- + K_k^x \big(y_k - C_k \hat{x}_k^-\big) \\ & X_k^x = \big(I - K_k^x C_k\big) X_k^{x^-}. \end{aligned} \tag{11}$$

Herein, the matrix $G_k^{x,w}$ represents the linear gain from the error variable ξ_k^w to the state estimation $\hat{x}_k$. Its actual definition is assessed by the following equality constraint, which is a vectorized representation of the dynamic system equation:

$$G_k^{x,w} \xi_{k-1}^w = \xi_{k-1}^A \hat{x}_{k-1} + \xi_{k-1}^B u_{k-1}. \tag{12}$$

Based on the introduced prediction and update algorithm, a reliable approximation of the governing state variables is determined, together with the corresponding uncertainty. This provides the foundation for a thorough study of the dynamical power assessment.

C. Power Flow Estimation

The convex mappings transform the dynamic model of the motor into an equivalent power flow-based representation, as the steady-state dissipation in the drive is approximated by a convex function of the output power flow. The instantaneous power flows in the system thus need to be assessed based on the obtained state estimates at each time instant. The input power of the drive is defined by the constant input voltage V^{dc} and the current drawn by the inverter i_k^{in} at time instant t_k

$$P_k^{\mathrm{in}} = V^{\mathrm{dc}} i_k^{\mathrm{in}}. \tag{13}$$

Denoting the actual estimation error on V^{dc} and i_k^{in} as ξ^V and ξ_k^i, one can rewrite this as a function of the estimates and the corresponding errors

$$P_k^{\mathrm{in}} = \big(\hat{V}^{\mathrm{dc}} + \xi^V\big)\big(\hat{i}_k^{\mathrm{in}} + \xi_k^i\big). \tag{14}$$

Grouping products of error variables in a single quadratic term consequently leads to

$$P_k^{\mathrm{in}} = \hat{V}^{\mathrm{dc}} \hat{i}_k^{\mathrm{in}} + \xi^V \hat{i}_k^{\mathrm{in}} + \hat{V}^{\mathrm{dc}} \xi_k^i + \mathcal{O}(\xi^2). \tag{15}$$

The inverter current i_k^{in} is related to the state variables via the Clarke transform [18] and the state of the discrete switches in the inverter x_k^b

$$\begin{aligned} i_k^{\mathrm{in}} &= {x_k^b}^T \begin{bmatrix} 1 & 0 & 0 & 0 \\ -\frac{1}{2} & \frac{\sqrt{3}}{2} & 0 & 0 \\ -\frac{1}{2} & -\frac{\sqrt{3}}{2} & 0 & 0 \end{bmatrix} \begin{bmatrix} i_k^{sx} \\ i_k^{sy} \\ \psi_k^{sx} \\ \psi_k^{sy} \end{bmatrix} \\ &\triangleq M_k^{i,x} x_k. \end{aligned} \tag{16}$$

The matrix $M_k^{i,x}$ is thus inherently defined as the transformation matrix from the state variables x_k to the inverter current i_k^{in}. In this formulation, the homopolar component of the current is assumed to be absent. Based on these considerations, (15) is reformulated into a notation containing only a dependence on quantities concerning the system variables V^{dc} and x_k. A recursive estimation is available for these variables

$$P_k^{\mathrm{in}} = \hat{V}^{\mathrm{dc}} M_k^{i,x} \hat{x}_k + \xi^V M_k^{i,x} \hat{x}_k + \hat{V}^{\mathrm{dc}} M_k^{i,x} \xi_k^x + \mathcal{O}(\xi^2). \tag{17}$$

On the other hand, the provided mechanical output power is expressed as a function of the torque and speed predictions, together with the corresponding instantaneous errors. The speed is assumed to be externally imposed by the driven load

$$P_k^{\mathrm{out}} = \big(\hat{T}_k + \xi_k^T\big)\big(\hat{\Omega}_k + \xi_k^\Omega\big). \tag{18}$$

The mechanical torque at time instant t_k is expressed as

$$T_k = \frac{3}{2} N_p \big(i_k^{sy} \psi_k^{sx} - i_k^{sx} \psi_k^{sy}\big). \tag{19}$$

A linearized equation in a confined neighborhood around the estimated variables is then determined

$$\begin{aligned} T_k = \frac{3}{2} N_p \big(&\hat{i}_k^{sy} \hat{\psi}_k^{sx} + \hat{i}_k^{sy} \xi_k^{\psi^{sx}} + \xi_k^{i^{sy}} \hat{\psi}_k^{sx} - \hat{i}_k^{sx} \hat{\psi}_k^{sy} \\ &- \hat{i}_k^{sx} \xi_k^{\psi^{sy}} - \xi_k^{i^{sx}} \hat{\psi}_k^{sy}\big) + \mathcal{O}(\xi^2). \end{aligned} \tag{20}$$

One can introduce the estimated torque $\hat{T}_k$, defined as

$$\hat{T}_k = \frac{3}{2} N_p \big(\hat{i}_k^{sy} \hat{\psi}_k^{sx} - \hat{i}_k^{sx} \hat{\psi}_k^{sy}\big). \tag{21}$$

Equation (21) is then reformulated into an equivalent vector representation

$$\begin{aligned} T_k &= \hat{T}_k + \frac{3}{2} N_p \begin{bmatrix} -\hat{\psi}_k^{sy} & \hat{\psi}_k^{sx} & \hat{i}_k^{sy} & -\hat{i}_k^{sx} \end{bmatrix} \xi_k^x \\ &\triangleq \hat{T}_k + M_k^{T,x} \xi_k^x. \end{aligned} \tag{22}$$

Substituting this in (18) leads to a tractable expression for the actual output power

$$P_k^{\mathrm{out}} = \hat{T}_k \hat{\Omega}_k + \hat{T}_k \xi_k^\Omega + M^{T,x} \xi_k^x \hat{\Omega}_k + \mathcal{O}(\xi^2). \tag{23}$$

The dissipated power flow P_k^d is given by the difference between input and output powers, independent of the direction of the power flow. The corresponding power loss is consequently written in a first-order approximation as

$$\begin{aligned} P_k^d = \hat{V}^{\mathrm{dc}} M_k^{i,x} \hat{x}_k + \xi^V M_k^{i,x} \hat{x}_k + \hat{V}^{\mathrm{dc}} M_k^{i,x} \xi_k^x \\ - \hat{T}_k \hat{\Omega}_k - \hat{T}_k \xi_k^\Omega - M^{T,x} \xi_k^x \hat{\Omega}_k + \mathcal{O}(\xi^2). \end{aligned} \tag{24}$$

The evolution of the dissipated power is, hence, directly correlated with the state estimations and the corresponding error variables. To alleviate the notation, the previous expression is symbolically rewritten into an equivalent formulation

$$P_k^d \triangleq \hat{P}_k^{\mathrm{in}} + \xi_k^{P_{\mathrm{in}}} - \hat{P}_k^{\mathrm{out}} - \xi_k^{P_{\mathrm{out}}} + \mathcal{O}(\xi^2). \tag{25}$$

The variables P_k^{in} and P_k^{out} denote the input and output power flows, respectively, and are thus defined as

$$P_k^{\mathrm{in}} = V^{\mathrm{dc}} i_k^{\mathrm{in}} \tag{26}$$

and

$$P_k^{\mathrm{out}} = T_k \Omega_k. \tag{27}$$

An appropriate power flow estimation is thus assessed based on the instantaneous state variables, determined using a modified Kalman filter on model expectations and sensor data. Nevertheless, the recursive convex mappings provide information with respect to steady-state dissipation at an averaged time scale, which can be evaluated based on the provided time evolution of the power flows. Averaged power quantities need to be consulted in an intelligent fashion to optimally update the motor loss mappings. The algorithmic procedure is schematically visualized in Fig. 3.

This article has been accepted for inclusion in a future issue of this journal. Content is final as presented, with the exception of pagination.

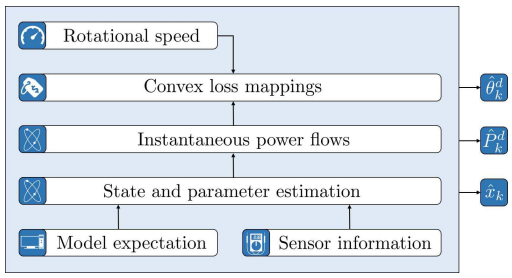

Fig. 3. General overview of the algorithmic structure.

III. Recursive Convex Loss Mapping Formulation

Energy-efficient operation is commonly a primordial objective in control systems concerning electric drives. The studied power losses do, therefore, constitute main decision criteria in the optimization of the system. In order to facilitate real-time execution of the control structures, the dissipated power in regime conditions can be approximated by a convex regression model in the provided output power, as power losses increase when deviating from optimal operation. A parabolic regression model with coefficients set $\theta = [\theta^{(1)}\ \theta^{(2)}\ \theta^{(3)}]^T$ proves to be sufficiently accurate from a control engineering perspective [12]. The elements of the vector θ represent the optimal quadratic approximation and are unknown variables that need to be estimated. A possible time dependence of the convex approximation is furthermore added in the framework. The corresponding time scale is nevertheless related to steady-state operation and is, therefore, denoted by the notation k'. A disturbance $d_{k'}$ with variance $D_{k'}$ represents the deviations from the expected quadratic trend and is assumed to be described as a Gaussian white noise

$$P_{k'}^d = \begin{bmatrix} P_{k'}^{\text{out}^2} & P_{k'}^{\text{out}} & 1 \end{bmatrix} \theta_{k'} + d_{k'}. \tag{28}$$

Introducing the appropriate error variable for the output power in the previous formulation leads to a first-order series in the estimation error, obtained by linearizing (28) around the expected operating point $\hat{P}_{k'}^{\text{out}}$

$$P_{k'}^d = \theta_{k'}^{(1)}\left(\hat{P}_{k'}^{\text{out}^2} + 2\hat{P}_{k'}^{\text{out}}\xi_{k'}^{P^{\text{out}}}\right) + \theta_{k'}^{(2)}\left(\hat{P}_{k'}^{\text{out}} + \xi_{k'}^{P^{\text{out}}}\right) + \theta_{k'}^{(3)} + d_{k'} + \mathcal{O}(\xi^2). \tag{29}$$

In which, the actual unknown mechanical power at the time scale k' was written as

$$P_{k'}^{\text{out}} = \hat{P}_{k'}^{\text{out}} + \xi_{k'}^{P^{\text{out}}}. \tag{30}$$

The quantities $\hat{P}_{k'}^{\text{out}}$ and $\xi_{k'}^{P^{\text{out}}}$ can herein be interpreted as an averaged representation of their respective counterparts in (25). In practical applications, the only available information concerning the power loss is incorporated in the regime dissipation estimate $\hat{P}_{k'}^d$, which is defined as

$$\hat{P}_{k'}^d = \hat{P}_{k'}^{\text{in}} - \hat{P}_{k'}^{\text{out}}. \tag{31}$$

Recalling (25), the estimate is reformed into a function of the actual dissipation and the error variables at the steady-state time scale

$$\hat{P}_{k'}^d = P_{k'}^d - \xi_{k'}^{P_{\text{in}}} + \xi_{k'}^{P_{\text{out}}} + \mathcal{O}(\xi^2). \tag{32}$$

Substituting (29) in this relation results in an expression linking the regression coefficients $\theta_{k'}$ to the available loss information source $\hat{P}_{k'}^d$

$$\hat{P}_{k'}^d = \theta_{k'}^{(1)}\left(\hat{P}_{k'}^{\text{out}^2} + 2\hat{P}_{k'}^{\text{out}}\xi_{k'}^{P^{\text{out}}}\right) + \theta_{k'}^{(2)}\left(\hat{P}_{k'}^{\text{out}} + \xi_{k'}^{P^{\text{out}}}\right) + \theta_{k'}^{(3)} + d_{k'} - \xi_{k'}^{P_{\text{in}}} + \xi_{k'}^{P_{\text{out}}} + \mathcal{O}(\xi^2) \tag{33}$$

and therefore,

$$\hat{P}_{k'}^d = \begin{bmatrix} \hat{P}_{k'}^{\text{out}^2} & \hat{P}_{k'}^{\text{out}} & 1 \end{bmatrix} \theta_{k'} + \left(1 + \begin{pmatrix} 2\hat{P}_{k'}^{\text{out}} & 1 & 0 \end{pmatrix} \hat{\theta}_{k'}\right) \xi_{k'}^{P_{\text{out}}} - \xi_{k'}^{P^{\text{in}}} + d_{k'} + \mathcal{O}(\xi^2). \tag{34}$$

A more structured notation can be engaged by introducing the corresponding linear gain factors

$$\hat{P}_{k'}^d \triangleq G_{k'}^{\theta}\theta_{k'} + G_{k'}^{\theta,P^{\text{out}}}\xi_{k'}^{P_{\text{out}}} + G_{k'}^{\theta,P^{\text{in}}}\xi_{k'}^{P_{\text{in}}} + d_{k'} + \mathcal{O}(\xi^2). \tag{35}$$

All error variables are directly correlated with the state and input deviations through expressions (17) and (23). The corresponding Kalman update procedure can then be initialized. The characteristic covariances of the distinct variables are symbolically represented by X. In the prediction step, the previous estimate is considered as the best guess for the innovated coefficients, as no significant dynamics are related to the regression model

$$\begin{aligned}
\textit{Prediction}\quad & \hat{\theta}_{k'}^- = \hat{\theta}_{k'-1} \\
& X_{k'}^{\theta^-} = X_{k'-1}^{\theta} \\
\textit{Update}\quad & R_{k'}^{\theta} = G_{k'}^{\theta} X_{k'}^{\theta^-} G_{k'}^{\theta^T} + G_{k'}^{\theta,P^{\text{out}}} X_{k'}^{P^{\text{out}}} G_{k'}^{\theta,P^{\text{out}^T}} \\
& \qquad + G_{k'}^{\theta,P^{\text{in}}} X_{k'}^{P^{\text{in}}} G_{k'}^{\theta,P^{\text{in}^T}} + D_{k'} \\
& K_{k'}^{\theta} = X_{k'}^{\theta^-} G_{k'}^{\theta^T} R_{k'}^{\theta^{-1}} \\
& \hat{\theta}_{k'} = \hat{\theta}_{k'}^- + K_{k'}^{\theta}\left(\hat{P}_{k'}^d - G_{k'}^{\theta}\hat{\theta}_{k'}^-\right) \\
& X_{k'}^{\theta} = \left(I - K_{k'}^{\theta} G_{k'}^{\theta}\right) X_{k'}^{\theta^-}.
\end{aligned} \tag{36}$$

In the practical implementation, the triple products in the different summations are calculated at each time instant t_k and averaged over a time interval $\Delta t' = t_{k'} - t_{k'-1}$ to obtain a reliable approximation of the steady-state operation. Procedure (36) is then initiated. A Kalman recursive update is elected as to facilitate the incorporation of stochastic variables, reflecting the reliability of the distinct information sources. The standard recursive least-squares algorithm [19] is, therefore, discarded.

IV. Discrete Information Extraction

The characteristic loss behavior of the drive system is strongly correlated with the rotational speed of the motor axis, incorporated in the dependence on the output power. Consequently, this relation needs to be reflected in the convex loss mappings and the quadratic regression models are, therefore, parametrized in the rotational speed [10]. Due to finite memory resources, convex approximations are only stored for an arbitrary set of discrete rotational speeds [10], [12]. Realistic applications are nevertheless characterized by a continuous variation in speed, as all possible values within

This article has been accepted for inclusion in a future issue of this journal. Content is final as presented, with the exception of pagination.

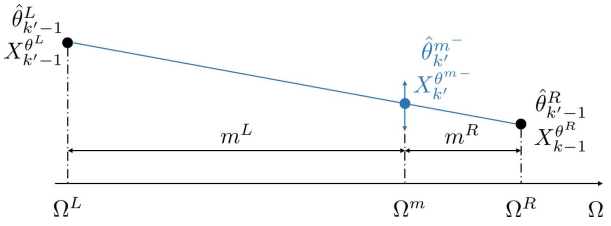

Fig. 4. Assessment of the characteristic parameters at the measured speed.

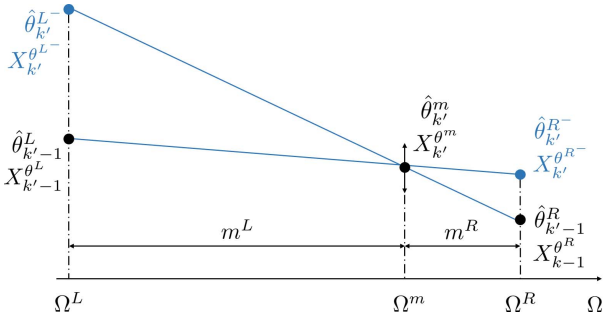

Fig. 5. Extrapolation of the obtained knowledge toward the stored data points.

the operating area can be achieved. Therefore, a heuristic needs to be constructed to extract valuable information from the continuously varying physical quantities and translate it to the discrete references. In the remainder of this paper, the rotational speed is assumed to be exactly known and consequently ξ_k^{Ω} equals zero at each time instant t_k. This corresponds to the situation, where a reliable measurement tool is equipped in the application resulting in only a minor uncertainty level on this variable.

A power estimation at a speed Ω^m is available at time instant $t_{k'}$, while the coefficient estimates and covariance estimations are stored for both neighboring speeds Ω^L and Ω^R. The reference speed Ω^L can, hereby, be interpreted as the nearest lower speed at which a mapping is stored. Similarly, Ω^R represents the closest higher neighboring speed with an associated regression model. The actual speed value Ω^m is thus contained in the interval $[\Omega^L, \Omega^R]$. In a first stage, an *a priori* prediction of the coefficient characteristics needs to be assessed at the intermediate speed, based on available information. The corresponding situation is schematically visualized in one dimension in Fig. 4.

As no knowledge of the behavior in between two discrete speeds is provided, the best *a priori* estimate consists of a linear interpolation between the neighboring vectors $\hat{\theta}^L_{k'-1}$ and $\hat{\theta}^R_{k'-1}$

$$\hat{\theta}^{m^-}_{k'} = \frac{m^R}{m^L + m^R}\,\hat{\theta}^L_{k'-1} + \frac{m^L}{m^L + m^R}\,\hat{\theta}^R_{k'-1}. \tag{37}$$

Deviations from the expected linear trend between two subsequent values of the speed are assumed to be reliably modeled as a white noise signal with variance Σ. The possibility of observing a considerable deviation is less pronounced close to Ω^R and Ω^L, as the original data are available in a close neighborhood of the considered point. Therefore, a parabolic uncertainty $E_{k'}$ is proposed

$$E_{k'} = \left(-\frac{4}{(m^L + m^R)^2} m^{L^2} + \frac{4}{m^L + m^R} m^L\right)\Sigma. \tag{38}$$

Based on the previous considerations, the covariance on the quadratic regression model at Ω^m is expressed as

$$X^{\theta^{m^-}}_{k'} = \left(\frac{m^R}{m^L + m^R}\right)^2 X^{\theta^L}_{k'-1} + \left(\frac{m^L}{m^L + m^R}\right)^2 X^{\theta^R}_{k'-1} + E_{k'}. \tag{39}$$

With the definition of these variables, the filter (36) can be executed. The estimate $\hat{\theta}^-_{k'}$ and the corresponding uncertainty measure $X^{\theta^-}_{k'}$ are hereby replaced by the previous expressions.

The recursive scheme then provides an innovated estimate of the coefficients and the covariance matrix. The resulting knowledge needs to be translated into an enhanced approximation at the outer bounds of the considered region, where the data are stored. Two primary estimates, $\hat{\theta}^{L^-}_{k'}$ and $\hat{\theta}^{R^-}_{k'}$, are computed, based on extrapolation of the previous parameters and the renewed information at the intermediary speed as demonstrated in Fig. 5.

The respective definitions of these predictions are, hence, given as

$$\hat{\theta}^{L^-}_{k'} = \frac{m^L + m^R}{m^R}\,\hat{\theta}^m_{k'} - \frac{m^L}{m^R}\,\hat{\theta}^R_{k'-1} \tag{40}$$

and

$$\hat{\theta}^{R^-}_{k'} = \frac{m^L + m^R}{m^L}\,\hat{\theta}^m_{k'} - \frac{m^R}{m^L}\,\hat{\theta}^L_{k'-1}. \tag{41}$$

Possible deviations from the proposed linear behavior, denoted by $E^L_{k'}$ and $E^R_{k'}$, are taken into account by reconsidering the proposed parabolic behavior of the uncertainty. A quadratic evolution is imposed in the interpolated areas, instead of the complete interval. In order to prevent the corresponding matrix to become negative, it is necessary to take the magnitude of the scaling factor. The additional extrapolation margin is then introduced as

$$E^L_{k'} = \left|-\frac{4}{m^{R^2}} m^{L^2} + \frac{4}{m^R} m^L\right|\Sigma \tag{42}$$

for the characteristic parameters at Ω^L and

$$E^R_{k'} = \left|-\frac{4}{m^{L^2}} m^{R^2} + \frac{4}{m^L} m^R\right|\Sigma \tag{43}$$

in the other case. The total uncertainty on the extrapolated predictions is then readily determined by summing the different contributions. For the lower bound in the speed region, Ω^L, this leads to

$$X^{\theta^{L^-}}_{k'} = \left(\frac{m^L + m^R}{m^R}\right)^2 X^{\theta^m}_{k'} + \left(\frac{m^L}{m^R}\right)^2 X^R_{k'-1} + E^L_{k'} \tag{44}$$

while the upper limit is characterized by

$$X^{\theta^{R^-}}_{k'} = \left(\frac{m^L + m^R}{m^L}\right)^2 X^{\theta^m}_{k'} + \left(\frac{m^R}{m^L}\right)^2 X^L_{k'-1} + E^R_{k'}. \tag{45}$$

The *a posteriori* estimate is chosen to be a weighted average of the prediction at the previous time instant $t_{k'-1}$ and the extrapolated prediction at t_k. In order to facilitate an analytical

This article has been accepted for inclusion in a future issue of this journal. Content is final as presented, with the exception of pagination.

solution, these variables are assumed to be uncorrelated. This does, however, not deteriorate the overall performance, as will be demonstrated in Section V.

$$\hat{\theta}^L_{k'} = \hat{\theta}^L_{k'-1} + K^L_{k'}\left(\hat{\theta}^{L^-}_{k'} - \hat{\theta}^L_{k'-1}\right)$$
$$\hat{\theta}^R_{k'} = \hat{\theta}^R_{k'-1} + K^R_{k'}\left(\hat{\theta}^{R^-}_{k'} - \hat{\theta}^R_{k'-1}\right). \quad (46)$$

For the first case, and given the assumption of being uncorrelated, the corresponding covariance matrix is formulated as

$$X^{\theta^L}_{k'} = \left(I - K^L_{k'}\right) X^{\theta^L}_{k'-1} \left(I - K^L_{k'}\right)^T + K^L_{k'} X^{\theta^{L^-}}_{k'} K^{L^T}_{k'} \quad (47)$$

and consequently

$$X^{\theta^L}_{k'} = K^L_{k'}\left(X^{\theta^L}_{k'-1} + X^{\theta^{L^-}}_{k'}\right) K^{L^T}_{k'} - K^L_{k'} X^{\theta^L}_{k'-1} - X^{\theta^L}_{k'-1} K^{L^T}_{k'} + X^{\theta^L}_{k'-1}. \quad (48)$$

This quadratic matrix equation is minimized if the following condition is fulfilled:

$$K^L_{k'} = X^{\theta^L}_{k'-1}\left(X^{\theta^L}_{k'-1} + X^{\theta^{L^-}}_{k'}\right)^{-1}. \quad (49)$$

The obtained outcome is intuitively interpreted as the matrix extension of a 1-D weighted average. If the initial uncertainty is large with respect to the extrapolated covariance, a significant importance is contributed to the updated data point stemming from the intermediate speed Ω^m. If the previous uncertainty is already at a relatively low level, no major adaptations are executed.

The methodology for the other component in (46) is completely analogous. The appropriate gain matrix $K^R_{k'}$ is given as

$$K^R_{k'} = X^{\theta^R}_{k'-1}\left(X^{\theta^R}_{k'-1} + X^{\theta^{R^-}}_{k'}\right)^{-1}. \quad (50)$$

The introduced definitions lead to a minimal covariance under the provided circumstances. The introduced heuristic should, therefore, provide reliable recursive modifications to the underlying power loss mapping, gradually improving the quadratic regression model up to the highest accuracy feasible in the considered system. This upper limit is imposed by distinct factors, e.g., sensor accuracy, number of stored data points, and so on.

V. Results and Discussion

The computational implementation of the previously introduced concepts is carried out in the MATLAB R2015b simulation environment. The underlying structure is highlighted in Fig. 6, in which a clear distinction is made between the simulation time scale Δt and the averaging horizon for the steady-state calculations $\Delta t'$. The simulation step Δt is fixed at 125 μs, whereas a single averaging horizon $\Delta t'$ has a duration of 0.5 s or equivalently 4000 time samples. The total time span of the simulation depends on the applied case study, as will be highlighted in an upcoming paragraph.

A certain speed profile is applied to the axis using an external drive, providing the necessary information concerning Ω^m over time. Reference values for the torque, T^{set}_k, are independently defined following a predefined load profile. Furthermore, three main decision criteria are visualized in the recursive procedure of Fig. 6. Startup of the machine is

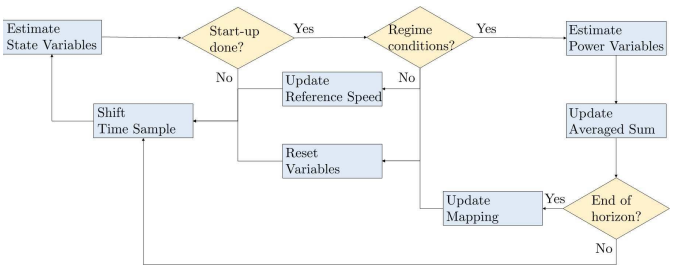

Fig. 6. Schematic overview of the adaptive convex mapping procedure in a simulation environment.

TABLE I
Nominal Values and Standard Deviations for the Stochastic Parameters in the Drivetrain

Parameter	Rated	σ	Parameter	Actual
$\hat{R}^s$	1.0676 Ω	$0.05\hat{R}_s$	R^s	1.0600 Ω
$\hat{R}^r$	0.4683 Ω	$0.05\hat{R}_r$	R^r	0.5121 Ω
$\hat{L}^s$	0.1414 H	$0.05\hat{L}_s$	L^s	0.1468 H
$\hat{L}^r$	0.1414 H	$0.05\hat{L}_r$	L^r	0.1468 H
$\hat{\kappa}$	0.9428	$0.02\hat{\kappa}$	κ	0.8940

arbitrarily chosen to be finished after 0.25 s, whereas electric regime operation is assumed to be attained after 0.1 s following a sudden change in the demanded power. A step in the imposed torque is defined as

$$\left|T^{\text{set}}_k - T^{\text{set}}_{k-1}\right| > 0.001 \text{ Nm}. \quad (51)$$

This constraint is, however, highly application dependent and constitutes a rigid boundary between disturbed and nondisturbed steady-state operation due to load changes. If the torque ramp would become too steep, regime operation is no longer a valid approximation and the associated mapping update would contain unreliable information.

A. Overview of the General Problem Characteristics

The considered case study is characterized by a constant deterministic dc source with a magnitude of 300 V ($\zeta^V = 0$). The control signals to the inverter gate drivers are provided by a direct torque control algorithm, relying on predefined look-up tables [20], with a constant flux reference Ψ^{set} equal to 0.75 Wb. Furthermore, an asynchronous machine with one pole pair is elected, for which the rated electric parameters are provided in the first column of Table I. These values are in realistic scenarios not exactly known and prone to uncertainty. The tolerance on the characteristics is assumed to be normally distributed around the nominal values with respective standard deviation σ. The fifth parameter L^m is hereby replaced by the dimensionless coupling factor κ, defined as

$$\kappa = \frac{L^{m^2}}{L^s L^r}. \quad (52)$$

The actual values for the distinct electric parameters, which are unknown, are randomly chosen from the resulting stochastic distributions. All numerical information concerning the induction motor is summarized in Table I.

This article has been accepted for inclusion in a future issue of this journal. Content is final as presented, with the exception of pagination.

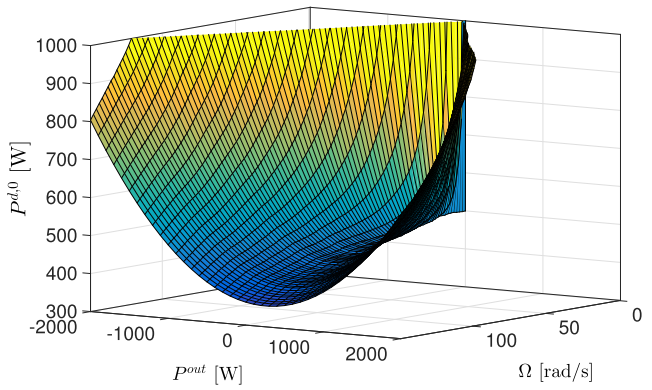

Fig. 7. Convex models of the initial power loss estimate $P^{d,0}$ as a function of the demanded output power P^{out} and the speed $\boldsymbol{\Omega}$.

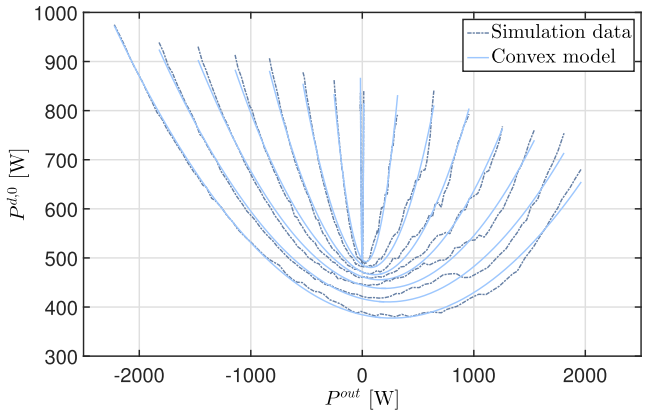

Fig. 8. Comparison of the regression model and the governing simulation data for an arbitrary selection of speeds. Wider parabolic curves correspond to higher rotational speeds.

Similar to [16], the initial covariance on the matrix elements is evaluated by taking an extensive amount of samples M in the distributions of the provided electrical parameters. The associated matrix models are then determined and translated into an equivalent vector representation w_0^i for each sample. The initial uncertainty on the model W_0 is thus defined as

$$W_0 = \frac{1}{M}\sum_{i=1}^{M}\left(w_0^i - \bar{w_0}\right)\left(w_0^i - \bar{w_0}\right)^T. \tag{53}$$

In this notation, the variable $\bar{w_0}$ is introduced to represent the average composition of the model parameter vector w_0.

In order to complete the overview of the general quantities in the simulated asynchronous drive, a concise review of the measurement (7) is still necessary. Sensor data are emulated by simulating the correct system, which are in practical applications not known, and consequently superposing a random error variable v_k. The error is supposed to be characterized by a normal distribution with covariance matrix V_k. In the numerical implementation, the measurement uncertainty is assumed to be fixed and characterized by

$$V_k = \begin{bmatrix} 0.01^2 & 0 & 0 \\ 0 & 0.01^2 & 0 \\ 0 & 0 & 0.01^2 \end{bmatrix} \quad \forall k. \tag{54}$$

The given numerical values are inspired by available information regarding the used sensor equipment. Stability of the proposed methodology under these conditions is not rigorously demonstrated but is verified based on numerous simulations. If the provided definition of W_0 is a reliable measure of the uncertainty on the different regression coefficients and their mutual dependence, the algorithm is observed to converge toward reliable estimates.

B. Initialization of the Convex Loss Mappings

Offline determination of the optimal quadratic coefficients for the different reference speeds relies on the dynamical model (5) and the given expected parameter values and associated standard deviations in Table I. No further information concerning the drive is initially known. A loss mapping is defined for all rotational speeds ranging from -1 to 149 rad/s, with a constant step of 2 rad/s. The optimal quadratic approximation is assessed by a standard least-squares algorithm, in which the quadratic error between the convex model and the reference data is minimized. These reference data are provided by short-term simulations of the system (5) at constant speed $\boldsymbol{\Omega}$, lasting 1 s with a simulation step of 125 μs. The simulation horizon is chosen long enough to guarantee that regime conditions are, in all scenarios, certainly achieved after half of the total time. The subsequent simulation data of the second half thus provide a trustworthy reflection of steady-state operation, as both stator and rotor time constants are significantly smaller than the considered time horizon. A list of 81 dynamic simulations is executed, for a uniform distribution of torque setpoints T^{set} in $[-17.5, 17.5\ \text{Nm}]$. The associated surface for the rated parameter values is visualized in Fig. 7. A smooth transition in the $\boldsymbol{\Omega}$-direction is observed, the associated regression model becomes broader for higher values of the rotational speed. At higher speeds, similar output power demands are associated with lower torques and thus lower dissipative losses.

The accuracy of the quadratic approximation is established in Fig. 8, in which the underlying simulation data used to construct the model is compared to the associated parabolic function. A close resemblance is observed, justifying the use of the proposed regression model for control purposes.

The proposed regression procedure is repeated $100\times$ for each discrete speed value with random combinations of parameter values selected from the corresponding normal distributions. This allows to evaluate the initial uncertainty on the coefficient set of the quadratic model X_0^θ in an empirical fashion. For a total of M_1 ($M_1 = 100$) samples, the respective definition of the covariance matrix is empirically given as

$$X_0^\theta = \frac{1}{M_1 - 1}\sum_{i=1}^{M_1}(\theta_i - \bar{\theta})(\theta_i - \bar{\theta})^T. \tag{55}$$

With $\bar{\theta}$ denoting the mean values for the quadratic coefficients over all conducted samples in the sample space. The

This article has been accepted for inclusion in a future issue of this journal. Content is final as presented, with the exception of pagination.

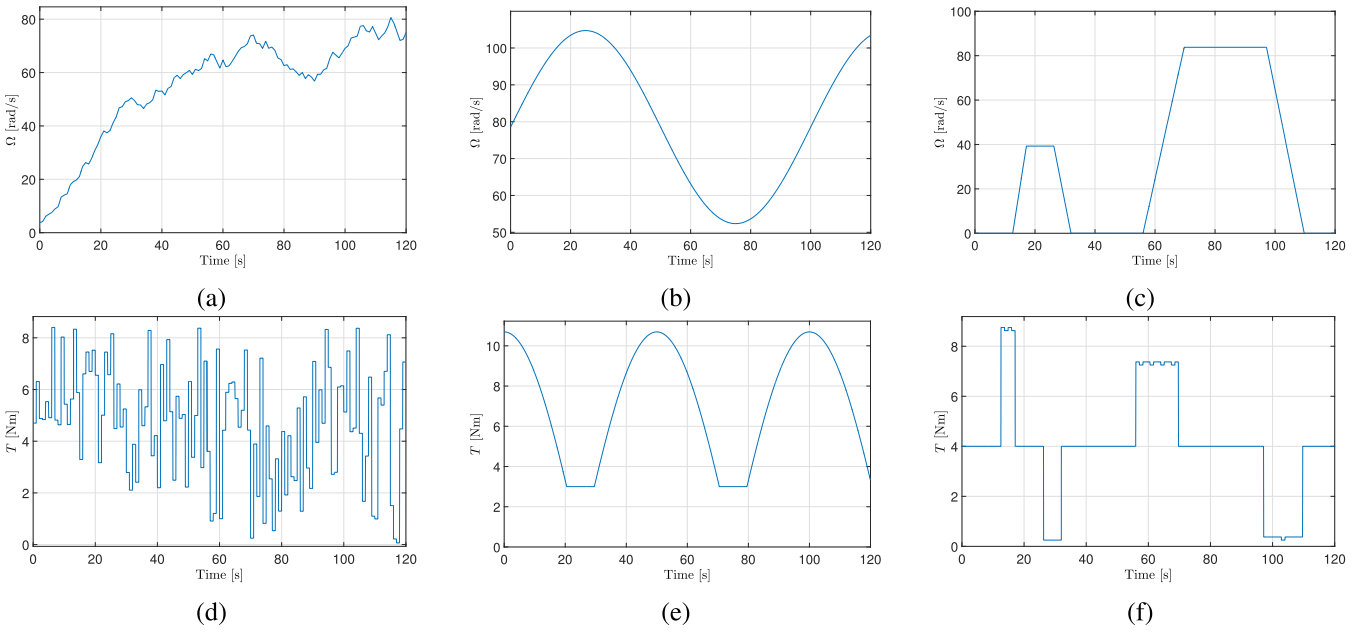

Fig. 9. Speed and torque evolution for the three reference scenarios. (a) Speed profile–random. (b) Speed profile–periodic. (c) Speed profile–drive cycle. (d) Torque profile–random. (e) Torque profile–periodic. (f) Torque profile–drive cycle.

characteristic covariances have to be assessed for each speed in the considered region of operating speeds.

Furthermore, an interpolation uncertainty Σ^l at the speed Ω^l, corresponding to the lth mapped speed, needs to be defined to quantify the introduced error due to linear interpolation for intermediate speeds. Suggesting the notation $\theta_i^{\Omega^l}$ for the regression coefficients at Ω^l of the ith conducted sample, facilitates expressing the associated interpolation covariance. The respective deviation δ_i^l is formulated as

$$\delta_i = \theta_i - \frac{\Omega^{l+1} - \Omega^l}{\Omega^{l+1} - \Omega^{l-1}} \theta_i^{\Omega^{l-1}} - \frac{\Omega^l - \Omega^{l-1}}{\Omega^{l+1} - \Omega^{l-1}} \theta_i^{\Omega^{l+1}} \tag{56}$$

and therefore,

$$\Sigma^l = \frac{1}{M_1 - 1} \sum_{i=1}^{M_1} \delta_i^l \, \delta_i^{l^T}. \tag{57}$$

These definitions are valid for the interpolation covariance at all intermediate reference speeds Ω^l. Recalling the information extraction at continuously variable speeds of Section IV, the general uncertainty matrix Σ [see (38)], can actually be defined as

$$\Sigma = \frac{m^R}{m^L + m^R} \Sigma^L + \frac{m^L}{m^L + m^R} \Sigma^R. \tag{58}$$

With identical notations as introduced in Section IV. If one of the enclosing bounds of the instantaneous speed consists of the lower or upper limit on the mapped rotational speeds, the appropriate formulation is, respectively, given as

$$\Sigma = \Sigma^R \tag{59}$$

or

$$\Sigma = \Sigma^L. \tag{60}$$

The covariance matrix $D_{k'}$ is finally assumed to be identically equal to zero, corresponding to an ideal underlying model exactly matching the parabolic dependence. Relation (28) is consequently fulfilled at each time instant $t_{k'}$ for a negligibly small disturbance $d_{k'}$. All necessary information to complete the representation of the system and enable the recursive update procedure (36) to be started, is hereby provided. Executing a single dynamic simulation of the system until regime conditions requires approximately 240 ms on a standard CPU. Initialization of the convex mappings thus requires preprocessing efforts for generating the various data points, resulting in a considerable relative time consumption. The associated mappings and uncertainty representation are nevertheless inherently coupled to the specific drive under study and the procedure has to be carried out only once before taking the considered component in operation.

C. Validation on Representative Trajectories

The performance of the introduced methodology involving adaptive convex loss mappings is numerically evaluated on multiple representative trajectories with their associated particularities in MATLAB R2015b. A certain speed profile is imposed to the axis of the drive and the resulting accuracy in loss assessment is determined. The first trajectory consists of a random behavior in speed and corresponding torque demands [Fig. 9(a) and (d)]. The randomized evolution allows to cover a large part of the operating region and validates the performance of the algorithm with respect to irregular behavior. Furthermore, a smooth sinusoidal speed evolution is imposed. The full range in operational speed is hereby analyzed, but the speed transitions are well defined, leading to smoothened power demands [Fig. 9(b) and (e)]. Finally, an automotive drive cycle-inspired trajectory is investigated,

This article has been accepted for inclusion in a future issue of this journal. Content is final as presented, with the exception of pagination.

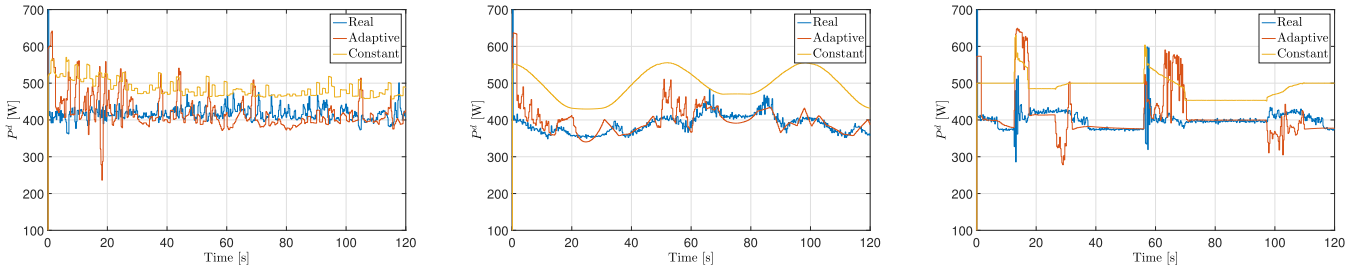

Fig. 10. Comparison of the loss prediction provided by a constant convex mapping and a recursively adaptable regression model for the three reference cases. (a) Random. (b) Periodic. (c) Drive cycle.

with significant sections at a constant speed. The associated profiles in rotational speed and torque are visualized in Fig. 9(c) and (f), respectively. Investigating the responses associated with the varying load cycles allows to validate the effectiveness of the numerical methodology in distinct operating environments, as the algorithm is ought to provide reliable estimates under all conditions.

The capability of the convex approximation to assess the losses in the drive is validated by rigorously comparing the difference in expected dissipated power at the considered speed proposed by the mapping $P_{k'}^{d,ad}$ and the actual power loss $P_{k'}^{d}$. This value is then compared to the performance of the initial convex regression models $P_{k'}^{d,0}$ in completely similar conditions. The real power loss $P_{k'}^{d}$, which functions as the reference scenario, is, hereby, calculated by employing the correct system parameters of Table I. The mathematical definition of the respective performance measures η^{ad} and η^{0} leads to

$$\eta^{ad} = \frac{1}{N'} \sum_{k'=1}^{N'} \left(P_{k'}^{d,ad} - P_{k'}^{d} \right)^2 \tag{61}$$

and

$$\eta^{0} = \frac{1}{N'} \sum_{k'=1}^{N'} \left(P_{k'}^{d,0} - P_{k'}^{d} \right)^2. \tag{62}$$

At specified time instants, uniformly distributed with a shift of 250 ms, the prediction error is evaluated, leading to a total of N' evaluations over the course of the total trajectory. The outcomes for the simulated responses and performance criteria in the three reference cases are summarized in Table II. It is important to note that the adaptive prediction corresponds to the situation, where the latest power flow estimation has not yet been accounted for. Hence, it can be considered as a reliable criterion in rigorously evaluating the generalized dissipated power prediction of the adapted mappings.

The corresponding evolution in time is depicted in Fig. 10. Based on the provided numeric results, it is observed that major increments in the loss assessment are obtained. The dynamic reconfiguration of the quadratic loss models enables to reduce the error on the loss prediction by a margin ranging from 55.7% to 89.0%, significantly outperforming the initial models. Slight deviations in performance are revealed

TABLE II
NUMERICAL RESULTS FOR THE THREE SIMULATED SCENARIOS

	Random	**Periodic**	**Drive cycle**
Duration	120s	120s	120s
Number of mapping updates	120	212	209
η^0	6055W^2	13320W^2	9776W^2
η^{ad}	2652W^2	1459W^2	4333W^2
Error reduction	56.2%	89.0%	55.7%

in the data of Table II, depending on the imposed speed and torque trajectories. Sudden transitions in the load induce swift variations in the power variables, slightly degrading the performance during these limited time intervals. Furthermore, regime conditions are regularly disturbed in this environment. Sinusoidal cycles are characterized by a smooth transition, without sudden steps in the load, and are, therefore, particularly suited for the iterative procedure. Moreover, all speeds in the operational range are obtained during only a brief period, allowing for significant initial adaptations. If a similar speed is maintained during extended time horizons, the uncertainty on the corresponding mappings is gradually decreased, resulting in only minor improvements. This phenomenon is observed in Fig. 10(c), in which several sections at a constant speed are incorporated in the trajectory. In each of the considered situations swift modifications are observed in the initial stages of the algorithm or for unseen speed regions. This is caused by the high initial uncertainty on the convex approximations, as the underlying electrical parameters are prone to significant deviations. Nevertheless, a noticeable improvement in loss assessing capabilities is still revealed and both the number and magnitude of the estimation peaks are diminished over time.

D. Experimental Validation

Previous results have been obtained based on virtual measurement data, solely relying on models and simulation data. Magnetic saturation, iron losses, and other undesired phenomena in electric machinery are, hereby, neglected, assuming a perfect analytical model and constant electrical parameters. In realistic scenarios, drift in parameter values may be observed due to temperature or saturation effects. Therefore, the proposed algorithm is validated on offline

This article has been accepted for inclusion in a future issue of this journal. Content is final as presented, with the exception of pagination.

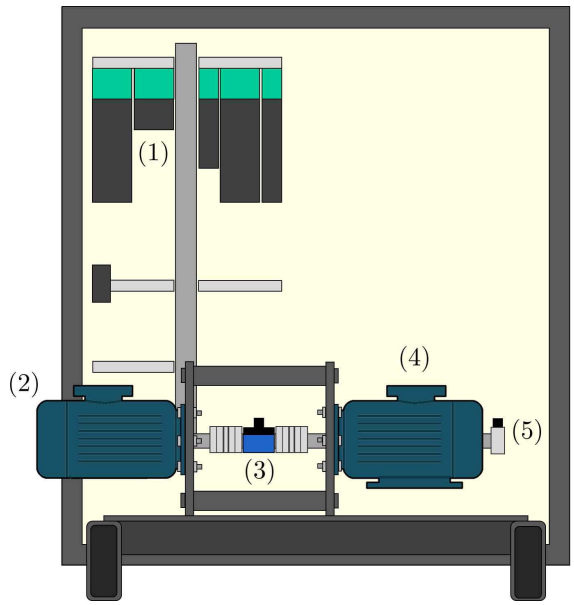

Fig. 11. Available lab equipment for collecting measurement data. (1) Industrial drive controls (2) Load motor in order to track the imposed reference speed of the drive. The rotational speed is measured by (5) incremental rotary encoder, while (3) torque transducer logs the exerted torque on the axis. (4) Controlled induction motor receives an arbitrary torque reference over time.

measurement data, in which these secondary phenomena are inherently present. The measurement data are collected using the experimental setup depicted in Fig. 11, for which the controlled motor has the same rated parameters as defined in Table I.

Supply to the controlled motor is provided by a dc voltage source at 300 V and an inverter, for which the corresponding voltage at the inverter side is monitored. Furthermore, the line current in the three phases $\hat{i}^s$ is measured. The stator voltage vector is denoted by $\hat{v}^s$. Control actions are executed using a dSpace DS1104 controller board. As the main objective is data collection, namely, currents, voltages, torque, and rotational speed, a flux estimator is implemented. To increase the robustness to deviations in the stator resistance, the standard integrator of the flux vector $\hat{\psi}^s$ is replaced with a discrete filter. A standard integrator would accumulate possible measurement offsets and an inaccurate knowledge of the stator resistance would furthermore lead to significant deviations at low-speed current or high load current. The flux vector is, therefore, estimated using a discretized low-pass filter, which is in fact the product of a regular integrator and an appropriate high-pass filter

$$\hat{\psi}^s_k = \frac{1}{1+\omega_c \Delta t}\hat{\psi}^s_{k-1} + \frac{\Delta t}{1+\omega_c \Delta t}\left(\hat{v}^s_k - \hat{R}^s \hat{i}^s_k\right). \qquad (63)$$

The cutoff frequency ω_c is empirically set at 2 rad/s and the time step Δt corresponds to the previously defined simulation step of 125 μs. This combination of values provides a satisfactory outcome in the experimental environment. The data are logged using dSpace ControlDesk and is then analyzed in an offline fashion. Hence, the secondary phenomena are inherently taken into account without having the need of a real-time implementation. Offline validation of the methodology is desired as an online execution would require a dedicated implementation on specialized platforms, e.g., field-programmable gate array units. As this is a challenging task on its own, the real-time execution and parallelization are the scope of future research. The primary goal of this paper is, therefore, restricted to demonstrating the applicability of the procedure on realistic scenarios.

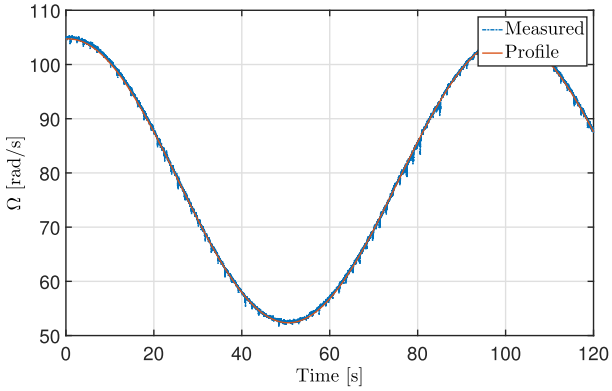

Fig. 12. Imposed speed profile and measured rotational speed.

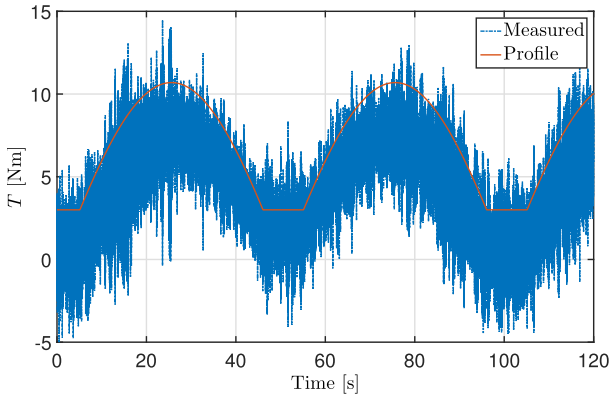

Fig. 13. Imposed torque reference profile and the measured total torque on the shaft.

The imposed speed and torque reference profiles are analogous to the periodic example provided in Section V-C and are depicted in Figs. 12 and 13 for enhanced clarity, together with the associated measurements.

No negative torque can be allowed for extended time intervals as the power flow is unidirectional. This explains the irregular shape of the periodic signals.

Torque and flux estimations, (21) and (63), respectively, are performed on the basis of the measured phase currents. The phase currents, together with the dc bus level, switching state, measured torque, and rotational speed are in a further stage analyzed to assess the performance of the adaptive mapping methodology. Based on the exported measurement data, a similar outcome is obtained with respect to the previously discussed simulation. The time evolution of the loss estimation is provided in Fig. 14. The associated numerical data are further specified in Table III. A total quadratic error reduction of 88.6% is observed with respect to the initially

This article has been accepted for inclusion in a future issue of this journal. Content is final as presented, with the exception of pagination.

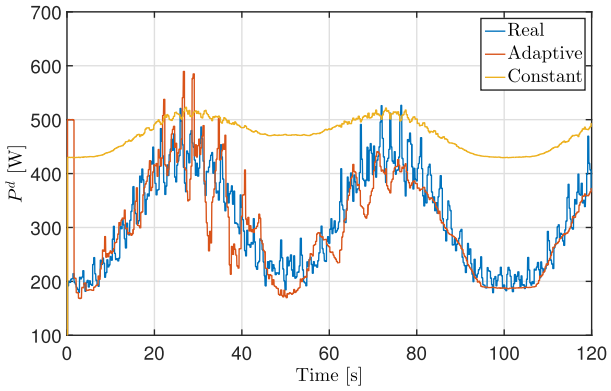

Fig. 14. Comparison of the loss prediction provided by a constant convex mapping and a recursively adaptable regression model for the measurement data.

TABLE III
NUMERICAL RESULTS FOR THE EXPERIMENTAL DATA

	Experimental
Duration	120s
Number of mapping updates	212
η^0	30019W^2
η^{ad}	3510W^2
Error reduction	88.6%

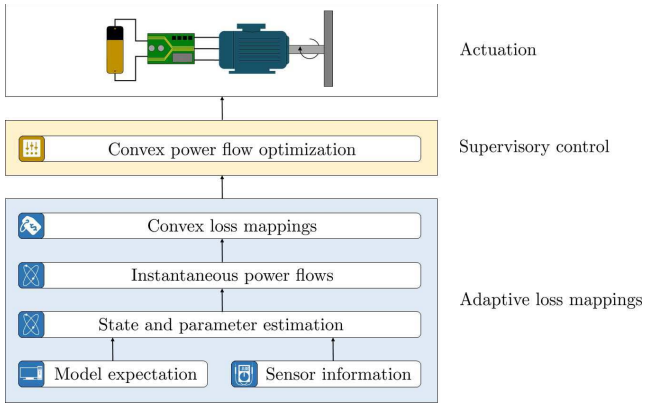

Fig. 15. Overview of a loss minimization procedure based on adaptive convex mappings in control applications.

generated convex mappings. Therefore, one can conclude that the performance of the algorithm is not significantly altered when exposed to realistic side effects as saturation and time dependencies. If additional sensing equipment is added to log the power flows at the inverter level, semiconductor losses could be experimentally introduced in the loss mappings, hereby further enhancing the accuracy of the dissipation models. This is, however, out of the scope of this paper and is the subject of future research.

The reliability of control decisions stemming from this information is, hence notably enhanced, possibly contributing to a more energy-efficient operation during runtime. Online adaptations furthermore permit applications in flexible environments as measurement information can be engaged to gradually adjust the current regression coefficients $\theta_{k'}$. The proposed methodology restricts the loss approximation to a quadratic model, hence maintaining the required convexity at each time instant. Supervisory control loops can thus still rely on time-efficient convex optimization procedures, in which the underlying quadratic models are recursively adapted to enhance the loss assessment when a dynamic load is exerted. No further modifications to the decision-making structure itself are, therefore, necessary. The adaptive coefficient estimation requires nevertheless a dedicated hardware implementation, but no additional sensing equipment needs to be added for this aim. A possible implementation of the introduced framework in a practical loss minimization scheme is carried out as schematically demonstrated in Fig. 15. The convex loss mapping supplies the control loop with information concerning the cost, i.e., dissipated energy of the associated control action.

VI. CONCLUSION

Optimal operation of practical electric drives is commonly characterized by the associated performance with respect to energy efficiency. Loss minimizing control algorithms at the system level provide the necessary control signals to guarantee an efficient operation in an online adaptive environment, as the governing operating conditions may be prone to temporal changes. Furthermore, due to the elevated complexity of contemporary drive systems, dedicated modeling formalisms are necessary to reduce the computational and algorithmic requirements. An adaptive convex loss mapping approach is introduced with the aim of combining flexibility and a reduced complexity in the supervisory control structures. Available model information, which is influenced by parameter uncertainty, and online measurement data are engaged to provide an optimal estimation of the power flows in the system. Accurate knowledge of the dissipated power and a corresponding uncertainty measure enable to dynamically reassess the most likely regression parameters of the convex loss model. As the corresponding mappings are stored at discrete speed values, an appropriate heuristic is deduced to facilitate the information extraction at arbitrary continues speed references. The viability of the introduced methodology is in this paper evaluated in a simulation environment and on experimental measurement data. Numerical results unveil the promising prospects of the considered approach, as the recursive loss assessment error is reduced by up to 89.0%, depending on the environmental conditions. Adaptive convex loss mappings can thus find a place in state-of-the-art control systems technology due to its appealing combination of a time-efficient format, enhanced loss assessment and flexibility to changing operating conditions. Nevertheless, future research should focus on efficient implementation of the proposed algorithmic approach, requiring more advanced and specialized computational platforms.

REFERENCES

[1] X. Hu, S. J. Moura, N. Murgovski, B. Egardt, and D. Cao, "Integrated optimization of battery sizing, charging, and power management in plug-in hybrid electric vehicles," *IEEE Trans. Control Syst. Technol.*, vol. 24, no. 3, pp. 1036–1043, May 2016.

This article has been accepted for inclusion in a future issue of this journal. Content is final as presented, with the exception of pagination.

[2] N. Murgovski, L. M. Johannesson, and J. Sjoberg, "Engine On/Off control for dimensioning hybrid electric powertrains via convex optimization," *IEEE Trans. Veh. Technol.*, vol. 62, no. 7, pp. 2949–2962, Sep. 2013.
[3] W. Xie, X. Wang, F. Wang, W. Xu, R. Kennel, and D. Gerling, "Dynamic loss minimization of finite control set-model predictive torque control for electric drive system," *IEEE Trans. Power Electron.*, vol. 31, no. 1, pp. 849–860, Jan. 2016.
[4] S. Sridharan and P. T. Krein, "Minimization of system-level losses in VSI-based induction motor drives: Offline strategies," *IEEE Trans. Ind. Appl.*, vol. 53, no. 2, pp. 1096–1105, Mar. 2017.
[5] L. Samaranayake and S. Longo, "Degradation control for electric vehicle machines using nonlinear model predictive control," *IEEE Trans. Control Syst. Technol.*, vol. 26, no. 1, pp. 89–101, Jan. 2018.
[6] P. M. Menghal and A. J. Laxmi, "Fuzzy based real time control of induction motor drive," *Procedia Comput. Sci.*, vol. 85, pp. 228–235, Jan. 2016.
[7] C. Vagg, S. Akehurst, C. J. Brace, and L. Ash, "Stochastic dynamic programming in the real-world control of hybrid electric vehicles," *IEEE Trans. Control Syst. Technol.*, vol. 24, no. 3, pp. 853–866, May 2016.
[8] M. Wieczorek and M. Lewandowski, "A mathematical representation of an energy management strategy for hybrid energy storage system in electric vehicle and real time optimization using a genetic algorithm," *Appl. Energy*, vol. 192, pp. 222–233, Apr. 2017.
[9] O. Sundstrom, L. Guzzella, and P. Soltic, "Torque-assist hybrid electric powertrain sizing: From optimal control towards a sizing law," *IEEE Trans. Control Syst. Technol.*, vol. 18, no. 4, pp. 837–849, Jul. 2010.
[10] B. Egardt, N. Murgovski, M. Pourabdollah, and L. J. Mardh, "Electromobility studies based on convex optimization: Design and control issues regarding vehicle electrification," *IEEE Control Syst.*, vol. 34, no. 2, pp. 32–49, Apr. 2014.
[11] A. De Keyser, M. Vandeputte, and G. Crevecoeur, "Convex mapping formulations enabling optimal power split and design of the electric drivetrain in all-electric vehicles," *IEEE Trans. Veh. Technol.*, vol. 66, no. 11, pp. 9702–9711, Nov. 2017.
[12] M. Vandeputte, A. De Keyser, and G. Crevecoeur, "Computationally efficient modeling for assessing the energy efficiency of electric drivetrains using convex formulations," *Int. J. Numer. Model.*, p. e2275, 2017. [Online]. Available: https://onlinelibrary.wiley.com/doi/full/10.1002/jnm.2275, doi: 10.1002/jnm.2275.
[13] F. Alonge, M. Cirrincione, F. D'Ippolito, M. Pucci, and A. Sferlazza, "Robust active disturbance rejection control of induction motor systems based on additional sliding-mode component," *IEEE Trans. Ind. Electron.*, vol. 64, no. 7, pp. 5608–5621, Jul. 2017.
[14] B. L. Boada, D. Garcia-Pozuelo, M. J. L. Boada, and V. Diaz, "A constrained dual Kalman filter based on pdf truncation for estimation of vehicle parameters and road bank angle: Analysis and experimental validation," *IEEE Trans. Intell. Transp. Syst.*, vol. 18, no. 4, pp. 1006–1016, Apr. 2017.
[15] M. Zorzi, "Robust Kalman filtering under model perturbations," *IEEE Trans. Autom. Control*, vol. 62, no. 6, pp. 2902–2907, Jun. 2017.
[16] A. De Keyser, D. Stroobandt, and G. Crevecoeur, "Adaptive state space representations enabling reliable and robust decision-making in asynchronous drives for mechatronic applications," in *Proc. IEEE Int. Conf. Adv. Intell. Mechatronics*, Munich, Germany, Jul. 2017, pp. 1501–1507.
[17] M. Barut, S. Bogosyan, and M. Gokasan, "Speed-sensorless estimation for induction motors using extended Kalman filters," *IEEE Trans. Ind. Electron.*, vol. 54, no. 1, pp. 272–280, Feb. 2007.
[18] S. Chattopadhyay, M. Mitra, and S. Sengupta, "Clarke and park transform," in *Electric Power Quality*. Dordrecht, The Netherlands: Springer, 2011. [Online]. Available: https://link.springer.com/book/10.1007/978-94-007-0635-4#about
[19] J. Voros, "Modeling and identification of Wiener systems with two-segment nonlinearities," *IEEE Trans. Control Syst. Technol.*, vol. 11, no. 2, pp. 253–257, Mar. 2003.
[20] C. M. F. S. Reza, M. D. Islam, and S. Mekhilef, "A review of reliable and energy efficient direct torque controlled induction motor drives," *Renew. Sustain. Energy Rev.*, vol. 37, pp. 919–932, Sep. 2014.

Arne De Keyser was born in Sint-Niklaas, Belgium, in 1993. He received the M.Sc. degree in electrical and mechanical engineering from Ghent University, Ghent, Belgium, in 2016, where he is currently pursuing his Ph.D. degree with the Department of Electrical Energy, Metals, Mechanical Constructions and Systems as a Ph.D. Student of the Special Research Fund (BOF). His current research interests include time-efficient optimization techniques of complex dynamic systems, focusing on real-time implementation of robust minimization strategies in electric drive systems.

Mr. De Keyser is an Affiliate Member of Flanders Make, the strategic research centre for the manufacturing industry in Flanders, Belgium.

Hendrik Vansompel was born in Lokeren, Belgium, in 1986. He received the master's and Ph.D. degrees in electromechanical engineering from Ghent University, Ghent, Belgium, in 2009 and 2013, respectively.

He is currently a Post-Doctoral Research Assistant with the Department of Electrical Energy, Metals, Mechanical Constructions and Systems, Ghent University. His current research interests include the design and control of electrical drives.

Guillaume Crevecoeur was born in 1981. He received the M.Sc. and Ph.D. degrees in engineering physics from Ghent University, Ghent, Belgium, in 2004 and 2009, respectively, where he joined the Department of Electrical Energy, Metals, Mechanical Constructions and Systems as a doctoral student in 2004. In 2009, he was a Post-Doctoral Fellow with the Research Foundation Flanders (FWO-Flanders). In 2011, he was a visiting researcher at the Technical University Ilmenau, Ilmenau, Germany, and the Physikalische Technische Bundesanstalt, Berlin, Germany. In 2014 he was appointed Associate Professor at the Faculty of Engineering and Architecture, Ghent University. His current research interests include the modeling, optimization and control of dynamical systems including foundational work on model-based optimization algorithms, inverse problems and nonlinear optimal control with strategic research on electromechanical and biomedical applications. Prof. dr. Crevecoeur is an Affiliate Member of Flanders Make, the strategic research center for the manufacturing industry.